Chemical Geology 332–333 (2012) 136–147

Contents lists available at SciVerse ScienceDirect

Chemical Geology

journal homepage: www.elsevier.com/locate/chemgeo

U–Th/Pb geochronology of detrital zircon and monazite by single shot laser ablation inductively coupled plasma mass spectrometry (SS-LA-ICPMS)

John M. Cottle *, Andrew R. Kylander-Clark, Johannes C. Vrijmoed [1]

Department of Earth Science, University of California, Santa Barbara, CA 93106, USA

ARTICLE INFO

Article history:
Received 8 May 2012
Received in revised form 19 September 2012
Accepted 22 September 2012
Available online 2 October 2012

Editor: L. Reisberg

Keywords:
U–Th/Pb geochronology
Zircon
Monazite
LA-ICP-MS

ABSTRACT

A modified single-shot laser ablation inductively coupled plasma mass spectrometry (SS-LA-ICPMS) technique is presented that enables rapid acquisition of in-situ U–Th/Pb dates on accessory minerals from a single laser pulse. Advances over existing techniques include formulation of a semi-automated data reduction method and robust error propagation. The effects of pulse-to-pulse laser stability and analyte transport configurations on the precision and accuracy of the analyses are systematically assessed. The validity of the SS-LA-ICPMS approach is demonstrated by repeat analyses of multiple zircon and monazite reference materials, which consistently reproduce to within uncertainty of accepted reference values. Application of the method to detrital zircon and monazite samples with a wide range of ages and variable parent and daughter nuclide concentrations results in U–Th/Pb age spectra that are statistically indistinguishable from conventional laser ablation protocols that employ continuous laser pulsing. The SS-LA-ICPMS technique is minimally destructive, offers increased sample and grain throughput and enables rapid dating of large numbers of grains—enabling, e.g., to identify grains that are geologically significant yet rare.

© 2012 Elsevier B.V. All rights reserved.

1. Introduction

In-situ uranium-lead geochronology of detrital zircon (e.g. Košler et al., 2002), and to a lesser extent other accessory phases such as monazite (Parrish, 1990) and rutile (Zack et al., 2011), has become a routine tool to determine a variety of tectonic and sedimentological parameters including provenance, maximum depositional age, and stratigraphic correlation. When combined with compositional data, detrital accessory-mineral age spectra have the potential to elucidate large-scale geologic problems including basin evolution and paleogeographic and tectonic reconstructions.

In detrital zircon studies, the short analysis time afforded by laser ablation inductively coupled plasma mass spectrometry (LA-ICPMS) compared with other geochronologic techniques (e.g. isotope dilution thermal ionization mass spectrometry (ID-TIMS) or secondary ionization mass spectrometry (SIMS)) is advantageous, enabling the analysis of large numbers of grains from many samples. High sample throughput is especially advantageous in studies that correlate stratigraphic units over long time intervals and/or assess fine-scale basin evolution.

In a similar manner, many detrital geochronology studies seek to identify the youngest grains within a sample to determine the maximum depositional age. Where the age of individual grains must be known to a high precision (e.g. volcanic ashes or stratigraphically important clastic sediments), grains can be extracted and analyzed after in-situ analysis to obtain high precision dates via ID-TIMS. This approach is particularly useful where the sub-population of interest (usually the youngest) may represent only a small percentage of grains.

In sum, further development of LA-ICPMS into a tool that can rapidly screen large numbers of grains and samples with minimal sample destruction has the potential to be useful in a wide variety of tectonic studies. In this contribution we present a method (modified from Cottle et al., 2009a) for detrital accessory phase U–Th/Pb geochronology that employs single-shot laser ablation multi-collector inductively coupled plasma mass spectrometry (SS-LA-ICPMS). A robust data reduction and error propagation method is described. The long-term accuracy and reproducibility of the method is assessed using multiple zircon and monazite reference materials. Analyses of natural detrital zircon and monazite samples demonstrate that the SS-LA-ICPMS method is capable of rapid and precise analysis of detrital accessory phases.

2. Background

Cottle et al. (2009a) presented a method in which zircons were ablated with an individual pulse of a solid-state 193 nm wavelength laser and analyzed using a Nu Plasma MC-ICPMS. That work demonstrated, through analysis of natural reference zircons, that it is possible to generate $^{206}Pb/^{238}U$ and $^{207}Pb/^{206}Pb$ ratios with external reproducibilities of 2% and 2.8% (2SD) respectively, using an amount of material similar to a conventional static ablation method. Reducing the amount of material ablated to ~25% of that consumed during their 'normal'

* Corresponding author.
E-mail addresses: cottle@geol.ucsb.edu (J.M. Cottle), kylander@geol.ucsb.edu (A.R. Kylander-Clark), Johannes.Vrijmoed@unil.ch (J.C. Vrijmoed).
[1] Now at: Institute de Minéralogie et Géochimie, University of Lausanne, CH-1015 Lausanne, Switzerland.

0009-2541/$ – see front matter © 2012 Elsevier B.V. All rights reserved.
http://dx.doi.org/10.1016/j.chemgeo.2012.09.035

ablation protocol resulted in a $^{206}Pb/^{238}U$ reproducibility of ~5% (2SD) while consuming ~14 ng zircon. In addition, by measuring successive laser pulses from a single ablation site, Cottle et al. (2009a) produced age-depth profiles through zircon crystals with a depth resolution of ~0.1 μm/pulse.

An analogous approach was taken by Johnston et al. (2009) using an Isoprobe MC-ICPMS (GV Instruments, U.K.) equipped with channeltron electron multipliers for detection of Pb signals. These authors employed continuous pulsing of the laser (either 40 or 32 pulses) and a total count integration method to sample volumes as small as 12–14 μm diameter and 4–5 μm deep (<3 ng of zircon).

In typical laser-ablation U–Pb geochronology studies (e.g. Jackson et al., 2001; Horstwood et al., 2003; Gehrels et al., 2008) isotope ratios are obtained by computing either the mean of the individual background-subtracted ratios that make up the measurement, or, by taking the ratio of the mean intensities. In contrast, in the single-shot method of Cottle et al. (2009a) a different approach was necessitated by the observation that, because of the mixed Faraday (^{238}U)/ion counter (^{206}Pb and ^{207}Pb) detector array employed, ratios generated from individual 200 ms integrations within a single pulse were both variable and inaccurate (see their Fig. 3). Cottle et al. (2009a) therefore integrated the total signal for each isotope over the entire pulse (from before shot baseline to after-shot baseline) generating a single isotope ratio from each pulse. This eliminated, to within analytical uncertainty of ~2%, any systematic offset that might result from either tau (decay) and/or response-time offset effects of the Faraday detectors relative to the ion counters. Pettke et al. (2011) adopted a similar approach to characterize fast transient signals and determine Pb isotope ratios from fluid inclusions, concluding that isotope ratios from fluid inclusions are best calculated using the bulk (total) signal integration technique.

In the method of Cottle et al. (2009a) the selection of both peaks and backgrounds was achieved manually in Excel. Repeat measurements of secondary reference materials were employed to estimate an analytical uncertainty. Here we present a new, semi-automated approach to data reduction and error propagation and demonstrate the accuracy and utility of this approach to detrital accessory phase mineral studies.

3. Methods

3.1. Instrumentation

Zircon and monazite were analyzed using a laser ablation multi collector inductively coupled plasma mass spectrometer (LA-MC-ICP-MS) system housed at the University of California, Santa Barbara (UCSB). Instrumentation, summarized in Table 1, consists of a 193 nm wavelength, 4 ns pulse-width ATL-Lasertechnik ArF Excimer laser ablation system (Photon Machines, San Diego, USA) coupled to a Nu Plasma MC-ICP-MS (Nu Instruments, Wrexham, UK). Analytical protocol is similar to that described by Cottle et al. (2009a) with three main modifications.

First, the collector arrangement on the Nu Plasma at UCSB allows for simultaneous determination of ^{232}Th and ^{238}U on high-mass side Faraday cups equipped with $10^{11}\Omega$ resistors and ^{208}Pb, ^{207}Pb, ^{206}Pb and ^{204}X (where X represents the isotopes of Pb and Hg) on four low-mass side ETP discrete dynode electron multipliers.

Second, in the setup adopted by Cottle et al. (2009a), a Tl–^{235}U solution was aspirated into the plasma during ablation to correct for instrumental mass bias and monitor plasma-induced inter-elemental fractionation. The collector configuration of the Nu Plasma at UCSB (see Table 1), precludes measuring Tl–^{235}U along with the Pb, U and Th isotopes; we therefore use a sample-standard bracket approach to correct for mass fractionation and instrumental drift.

Finally, Cottle et al. (2009a) employed a UP193SS 193 nm solid-state laser ablation system equipped with an in-house low volume (~3 cm^3) teardrop ablation cell capable of holding one 25 mm diameter epoxy disc of unknowns and one 6 mm epoxy disc of reference materials.

Table 1
Instrument parameters.

Nu Instruments 'HR Nu Plasma' MC-ICPMS	
Carrier gas and flow rate	0.25 l min^{-1} (He) + 0.98 l min^{-1} Ar makeup from onboard mass flow controllers. Ar added half way between the cell and the torch via 'T'-piece or mixing bulb (see text for further details)
Auxiliary gas flow rate	0.8 l min^{-1} (Ar)
Cool gas flow rate	13 l min^{-1} (Ar)
RF power	1300 W
Reflected power	<1 W
Sample cone	Ni (1 mm orifice)
Skimmer cone	Ni (0.7 mm orifice)
Collector types	2 Faradays and 4 electron multipliers
Integration times	200 ms
Isotopes measured	$^{204}Hg + Pb$, $^{206, 207, 208}Pb$ on SEMs; ^{232}Th, ^{238}U on Faraday cups
Reference Materials	91500 (1065 ± 0.4 Ma) Plesovice (337.13 ± 0.37 Ma) GJ1 (601.7 ± 1.3 Ma)
Photon Machines 193mn ArF excimer laser	
Cell	Two volume Helex cell (Eggins et al., 1998; Eggins et al., 2005)
Sample transport tubing	0.5 m length, Teflon
Washout time[a]	<1 s
Wavelength	193 nm ArF
Fluence	2.7–3.1 J cm^{-2}
Pulse width	<3 ns @ 1064 nm
Cell volume	3 cm^3
Drill depth/pulse	0.13 um @ 35 um diameter spot (50% power)

[a] Time taken for signal to reduce to 1% of peak intensity.

The laser ablation system at UCSB is equipped with a two-volume 'HelEx' ablation cell modified from the design of Eggins et al. (1998, 2005). The cell holds up to 9 × 25 mm diameter epoxy resin discs (or 3 × 25 mm discs and 4 normal size petrographic thin sections) and 2 × 10 mm epoxy discs containing reference materials. With the UPS1933SS, ablation occurred in an He atmosphere with Ar added approximately half way between the cell and the torch using a glass mixing bulb. In the UCSB system, the He gas flow to the main cell is adjusted independently of the He flow to the inner ablation cup, resulting in the efficient removal of analytes from the ablation site to the mass spectrometer. This design also facilitates a rapid washout, with a 99% reduction in peak signal in < 1 s.

In this study we applied two separate ablation protocols. The first represents a typical approach for our LA-ICPMS setup using a spot diameter of 24 μm (zircon) or 7 μm (monazite), a frequency of 4 Hz (for a 30-second total of 120 shots) and 2.7 J/cm^2 fluence (measured at the sample surface) at a laser energy of 4 mJ (operated in a constant-energy mode). This results in craters that are typically 7 μm deep. The measurement consists of two initial laser pulses to remove surface contamination, followed by a 10-second washout of the surface material, and then 25 s of continuous pulsing during which data are collected. After a 3 second wait, the next analysis commences, thus there is a total wait time between analyses of 13 s. This protocol was employed to provide a baseline comparison of the accuracy and precision of the SS-LA-ICPMS method when applied to detrital zircon and monazite samples.

In the 'single shot' LA-ICPMS (SS-LA-ICPMS) method, the laser was fired once every 10 s then moved to the next sample location (equivalent of 0.1 Hz repetition rate) at 3.1 J/cm^2 fluence (measured at the sample surface) at a laser energy of 5 mJ (operated in a constant-energy mode) and a spot size of 31 μm (zircon) or 8 μm (monazite). The laser ablation rate was measured at 95–120 nm/pulse using a scanning electron microscope (SEM). Prior to each SS-LA-ICPMS analytical run all samples and reference materials are ablated with two shots of the laser to remove surface contamination—although recorded, these data are discarded from final age calculations.

3.2. Sample preparation

Zircon and monazite separates were prepared using standard crushing and heavy liquid separation techniques. To minimize any potential sampling bias, an aliquot of 500–2000 grains from the bulk separates were mounted (without magnetic separation or hand picking) directly into 25 mm diameter epoxy resin discs and polished. All zircons were mapped using a cathodoluminescence imaging system attached to a FEI Q400 FEG scanning electron microscope (SEM) at the University of California, Santa Barbara. Monazites were imaged with backscattered electron on the same instrument. The SEM was operated at 10 kV accelerating voltage and a beam current of 0.5 nA. In an attempt to minimize the presence of any surficial common lead, prior to isotopic analysis, reference materials and unknowns were placed in an ultrasonic bath in high purity water then washed in alcohol, 2% nitric acid and finally in high purity water.

3.3. Data reduction

For the conventional ablation protocol, data reduction, including corrections for baseline, instrumental drift, mass bias and down-hole fractionation was carried out using Iolite version 2.1.5. Full details of the data reduction methodology can be found in Paton et al. (2010); in brief, background intensities and changes in instrumental bias were interpolated using a smoothed cubic spline while down-hole inter-element fractionation was modeled using an exponential function. The data reduction strategy and software developed for SS-LA-ICPMS is outlined in detail below. In both cases, $^{207}Pb/^{235}U$ ratio was calculated using the measured $^{206}Pb/^{238}U$ and $^{207}Pb/^{206}Pb$ ratios multiplied by the $^{238}U/^{235}U$ constant (137.88; Steiger and Jäger (1977)). All ages in this study were calculated using the U decay constants of Jaffey et al. (1971) and the Th decay constant of Amelin and Zatisev (2002). All uncertainties are quoted at the 95% confidence or 2σ level. Concordia diagrams were constructed using Isoplot 3.75 (Ludwig, 2012).

Cottle et al. (2009a) used a simple Excel worksheet to calculate total-signal intensities. This is time intensive, requiring manual selection of many peaks (a typical analytical run for a detrital sample consists of 120 unknowns bracketed by 39 primary and secondary reference material analyses). It also required a subjective assessment of where the signal ended and where the background began in order to make a baseline subtraction and calculate the total signal. To avoid this issue and enable efficient data reduction, a new MatLab code, *SLaPChron*, was constructed that automatically identifies the baseline and the peaks, calculates total counts, performs corrections for mass bias and instrumental drift, normalizes the unknowns to a primary reference material and calculates ages (Online Appendix 1, Fig. 1).

The input file consists of a comma-separated file containing isotope intensities for each collector in 200 ms time intervals. The user must also provide the number of analyses contained within the file, the name of the primary reference material being employed and identify the relative position of analyses of the primary reference materials in the file. In brief, the program first converts ^{238}U and ^{232}Th voltages (measured on Faraday cups) to counts, it then computes the mean intensity for each isotope throughout the entire run in counts. This is

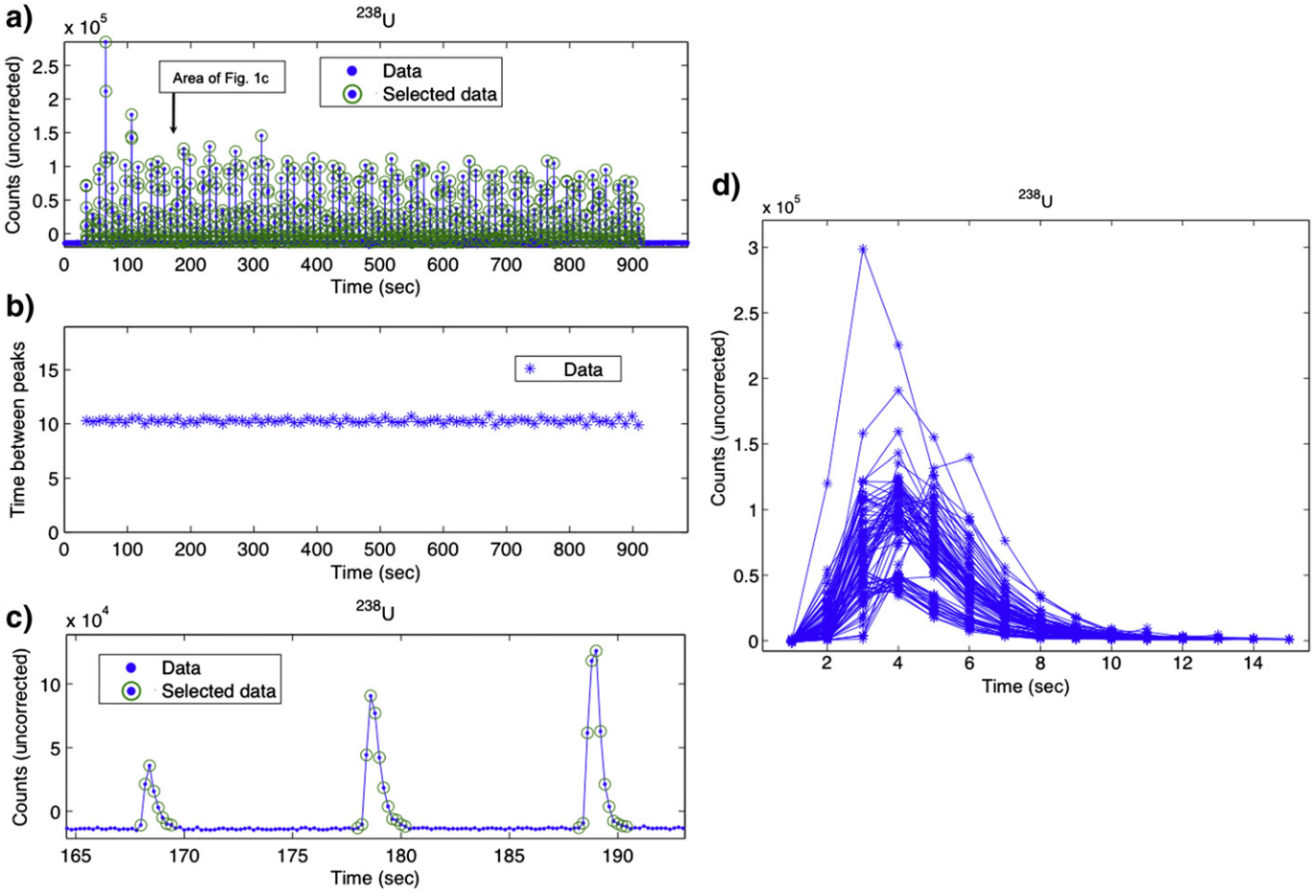

Fig. 1. Typical graphical output from the *SLaPChron* data-reduction program. a) Raw ^{238}U counts showing all data (blue asterisks) and points selected automatically to define each peak (open green circles), b) calculated time between each analysis, used in peak hunting routine to determine ion counter trips (see text for further details), c) inset showing three individual peaks, and d) all analyses from one analytical run stacked for visual comparison.

used as an initial threshold value above which points are considered to be analyses (as opposed to background). For peaks that are far above background and of equal magnitude this can be a sufficient criterion to identify all analyses. However, because the standard deviation of the mean isotope intensity is typically large (e.g. in the case of detrital samples), this method does not detect all of the analyses (the total number of which is specified by the user) in some cases. The mean threshold value is therefore automatically lowered or raised (the latter is sometimes necessary when many small peaks are identified leading to a detection of too many peaks) accordingly, with step size equal to the standard error of the total background between the peaks identified in the first step, until the number of detected peaks matches the number of user specified analyses (Fig. 1a). In addition, the algorithm assesses the time interval between all detected peaks, and detects outliers below the median value (approximating the time spacing between analyses) (Fig. 1b) which enables the detection of ion-counter trips resulting from ion-beams $>2e^6$cps. The iteration finishes when all missed peaks are detected. All of the peak three standard deviations below the median value are rejected, removing all minor or secondary peaks on the tails of the main analyses.

Secondly, the program calculates a mean and standard deviation of the background between the detected peaks. Each peak is then traced from the top down to include each datum above the mean value plus a user-specified number of standard deviations of the background on either side of the peak (2 SD in this study). A final datum in front of each peak is added, to be certain that the rapid rise at the start of the analysis is captured (it is possible that when the first datum of an analysis is detected, the signal will already be significantly above background and thus those counts might be ignored) (Fig. 1c). The points that remain after peak selection are considered background; the mean of these values is then linearly interpolated to obtain an approximate value at each integration point constituting the peak. Any inaccuracy attributable to identifying the correct baseline values contributes minimal uncertainty because the total number of counts under the peak is summed.

Unknowns and reference materials are identified by their user-defined position within the run. The integration of each peak is then a simple sum of all counts beneath the peak (Fig. 1d). Isotope ratios are calculated by dividing the total number of counts for each isotope under the peak. Corrections for laser-induced fractionation, mass bias and instrumental drift employ a sample-standard bracket approach. The measured ratio for each primary reference material is divided by the appropriate known (ID-TIMS) value to obtain a correction factor that accounts for laser-induced (inter-)elemental fractionation and/or instrumental mass bias. The correction factor is linearly interpolated throughout the run and applied to each unknown and secondary reference material at the appropriate time-slot. The normalized isotope ratios are then used to calculate ages.

Elemental U, Th and Pb concentrations are calculated using a sample-standard bracket approach in which a correction factor is obtained by dividing the total counts of U, Th and Pb measured in the matrix-matched primary reference material by the known value. A linear regression is calculated for the entire run and the correction factor at the appropriate time-slot is then applied to each of the unknowns and secondary reference materials.

As with the method of Cottle et al. (2009a) any inaccuracy in measured isotopic ratios produced by differential detector response–and any need for a tau correction–is avoided by summing the total number of counts under the curve.

3.4. Error propagation

Each measurement with SS-LA-ICP-MS method consists of only a single intensity for each isotope; it is therefore not possible to produce an internal uncertainty for each datum based on the standard error of the mean ratio or mean intensity as is done in conventional LA-ICPMS analyses. We identify four main sources of uncertainty that need to be accounted for: 1) the uncertainty in relevant decay constants; 2) the uncertainty in the accepted value of the primary reference material; 3) the 'internal' counting statistics uncertainty associated with the individual measurement and; 4) the 'external' uncertainty or, the additional uncertainty required to make each datum comparable to another datum run in the same, or a different analytical session. The uncertainties in λ_{238}, λ_{235} and λ_{232} are treated as systematic errors and therefore not propagated into individual unknown analyses. Sources 2) and 3) can be quantified and added in quadrature to give an approximation of the internal uncertainty. One approach to calculating the external uncertainty is to measure a series of secondary reference materials analyzed concurrently with unknowns and compute the external uncertainty required to produce a single population for the secondary reference material. This can be achieved using a Maximum-Likelihood Estimation (MLE) method, assuming a Gaussian distribution of errors and a Student's-*t* multiplier for $2N-2$ degrees of freedom (see Ludwig, 2012 for further details). This minimum uncertainty can then be quadratically added to the internal uncertainty of each datum to produce the external uncertainty.

An alternative approach is to take the relative standard deviation (RSD) of the $^{207}Pb/^{206}Pb$, $^{206}Pb/^{238}U$, and $^{208}Pb/^{232}Th$ ratios of the primary reference material (that pass a 2-sigma outlier rejection test) for a given analytical session and quadratically add this uncertainty to each unknown and secondary reference material. Fig. 2 plots the 2-sigma uncertainty calculated using both the MLE and RSD methods for twenty randomly selected analytical sessions. Both methods yield a similar uncertainty, suggesting that the 2RSD uncertainty adequately captures the external uncertainty. We adopt the latter, RSD, method because unlike the MLE method it does not require measurement of multiple secondary and tertiary reference materials.

The uncertainties for ratios and concentration data are calculated using the following formulae, where σ is the uncertainty of the ratio R ($R638 = {}^{206}Pb/^{238}U$, $R76 = {}^{207}Pb/^{206}Pb$, $R832 = {}^{208}Pb/^{232}Th$) or concentration, mprm is the measured standard deviation of the primary reference material (after 2 sigma outlier rejection), and cs_{meas} is the counting statistics uncertainty on the measured ratio or concentration. The uncertainty on each of the ratios and concentration measurements is equal to the quadratic sum of 2RSD of the primary reference material for that session and the counting statistics uncertainty:

$$\sigma_{R638} = \sqrt{\left(\sigma R638_{mprm}\right)^2 + \left(\sqrt{\frac{206cs_{meas}}{238cs_{meas}}}\right)^2} \quad (1)$$

$$\sigma_{R76} = \sqrt{\left(\sigma R76_{mprm}\right)^2 + \left(\sqrt{\frac{207cs_{meas}}{206cs_{meas}}}\right)^2} \quad (2)$$

$$\sigma_{R832} = \sqrt{\left(\sigma R832_{mprm}\right)^2 + \left(\sqrt{\frac{208cs_{meas}}{232cs_{meas}}}\right)^2} \quad (3)$$

$$\sigma_{U} = \sqrt{\left(\sigma U_{mprm}\right)^2 + \left(\sqrt{U8cs_{meas}}\right)^2} \quad (4)$$

$$\sigma_{Th} = \sqrt{\left(\sigma Th_{mprm}\right)^2 + \left(\sqrt{Th2cs_{meas}}\right)^2} \quad (5)$$

$$\sigma_{Pb} = \sqrt{\left(\sigma \sum \left(206Pbcs_{mprm} + 207Pbcs_{mprm} + 208Pbcs_{mprm}\right)\right)^2 + \left(\sqrt{\sum \left(206Pbcs_{meas} + 207Pbcs_{meas} + 208Pbcs_{meas}\right)}\right)^2}. \quad (6)$$

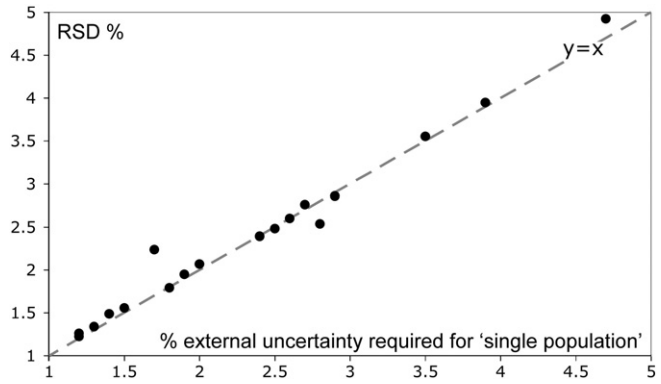

Fig. 2. 2-Sigma uncertainty (in percent) calculated using both the maximum-likelihood estimation (MLE) method and RSD methods for twenty randomly selected analytical sessions. Both methods yield a similar uncertainty, suggesting that the 2RSD uncertainty adequately captures the required external uncertainty.

4. Results

4.1. Laser stability

During the course of this study we observed that the first few analyses of a given run often displayed significantly variable intensities and ratios, independent of the apparent stability of the mass spectrometer (as assessed by repeat solution measurements). To investigate the potential causes of this, we performed a series of experiments to establish the energy stability of the laser ablation system and whether this affects the precision and/or reproducibility of the analyses. Fig. 3 displays the results of two such experiments in which the laser was fired once every 10 s for ~60 min (1 second firing time + 10 second wait = 325 shots over 1 h) to simulate a typical analytical run. Laser energy was measured at the sample surface using a Gentec SOLO 2™ energy monitor. Time-stamped data were automatically recorded using the built-in software.

These experiments demonstrate two types of behavior (illustrated by representative examples in Fig. 3), in which over the first 60 pulses (~11 min), the energy output of the laser either increases or decreases before stabilizing around a mean value. In the illustrated cases, the energy increases or decreases by 17% or 14% respectively (maximum/minimum values relative to the mean). After about pulse number 60, the laser energy stabilizes such that the individual laser pulse energy is reproducible to 8.2% and 8.5% (2 RSD), respectively. Repeating this experiment with different wait times between pulses demonstrates that it is the number of shots rather than the time elapsed since the first shot that determines when the laser energy stabilizes. In all subsequent analytical sessions we therefore fired the laser ~100 times behind the shutter to stabilize the energy output before beginning the analyses.

A second set of experiments was conducted to assess the affect of pulse-to-pulse laser stability on both ablation yield and inter-element fractionation. The ATL laser system was modified to record the energy output of the laser for each single pulse analysis such that each analysis can be directly related to an energy value at the time of ablation. The laser energy was systematically increased from 3.5 mJ to 5.5 mJ while repeatedly analyzing GJ-1 zircon. Fig. 4 demonstrates that although the ablation yield increases with increasing laser energy (as assessed by increasing total U counts, Fig. 4a), the $^{206}Pb/^{238}U$ ratio does not change appreciably—i.e. the value and reproducibility of the $^{206}Pb/^{238}U$ ratio is similar when the energy is varied (pulses 1–110, Fig. 4) and at constant energy (pulses 110–150, Fig. 4). We therefore infer that any minor variations in laser energy do not significantly contribute to the 'within session' uncertainty obtained from repeat isotopic ratio measurements of a reference material.

4.2. Analyte transport

In the original single-shot contribution by Cottle et al. (2009a) the analyte was transported from the laser ablation cell to the ICP via a 2.3 m long Teflon-lined Tygon® tube with Ar (and a Tl–^{235}U monitor solution) mixed at a 'T'-junction approximately 1 m from the torch. To investigate whether different tubing configurations resulted in a better signal-to-noise ratio, increased signal size or better signal stability, four different setups were tried. In the first case, Ar was added to the analyte + He mixture at a Teflon T-joint approximately ~20 cm (half way) between the outlet of the cell and the ICP torch. In the second case, Ar was added to the analyte + He mixture in a glass mixing bulb (a 25 mm diameter × 70 mm glass cylinder that promotes turbulent flow during addition of the Ar make-up gas) approximately ~20 cm (half way) between the outlet of the cell and the ICP torch. The above two configurations were further modified by the addition of 5 m of Teflon-lined Tygon® tubing between the Ar input and the torch.

Fig. 5 displays the mean values of 10 repeat ablations of the GJ-1 reference zircon using the four different configurations. In each case, the laser was fired at the 1.0-second point. The T-junction resulted in the narrowest signal profile, reflecting limited mixing of the analyte prior to the torch. Use of the mixing bulb resulted in a slight broadening of the signal; adding 5 m of tubing to this led to a significant tailing of the peak, with a possible secondary 'peak' at approximately 6 s. The tailing of the peak observed with the 5 m of additional Tygon tubing could, in

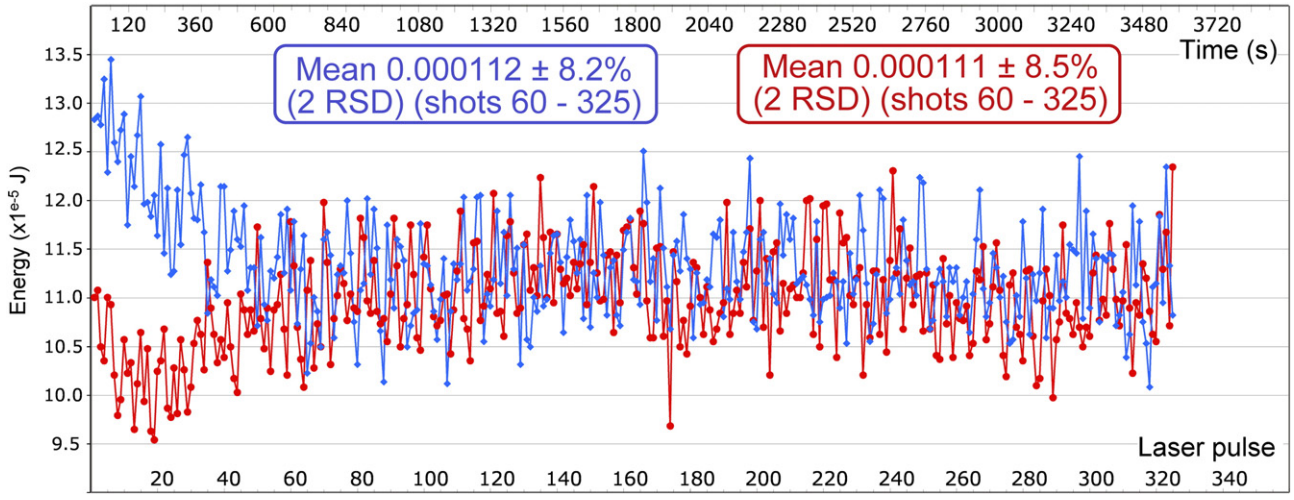

Fig. 3. Laser energy measured at the sample surface for two 60 minute experiments in which the laser was fired once every 10 s (1 second firing time + 10 second wait = 325 shots over 1 h) to simulate a typical analytical run. The laser energy at the sample surface stabilizes after 50–60 individual shots.

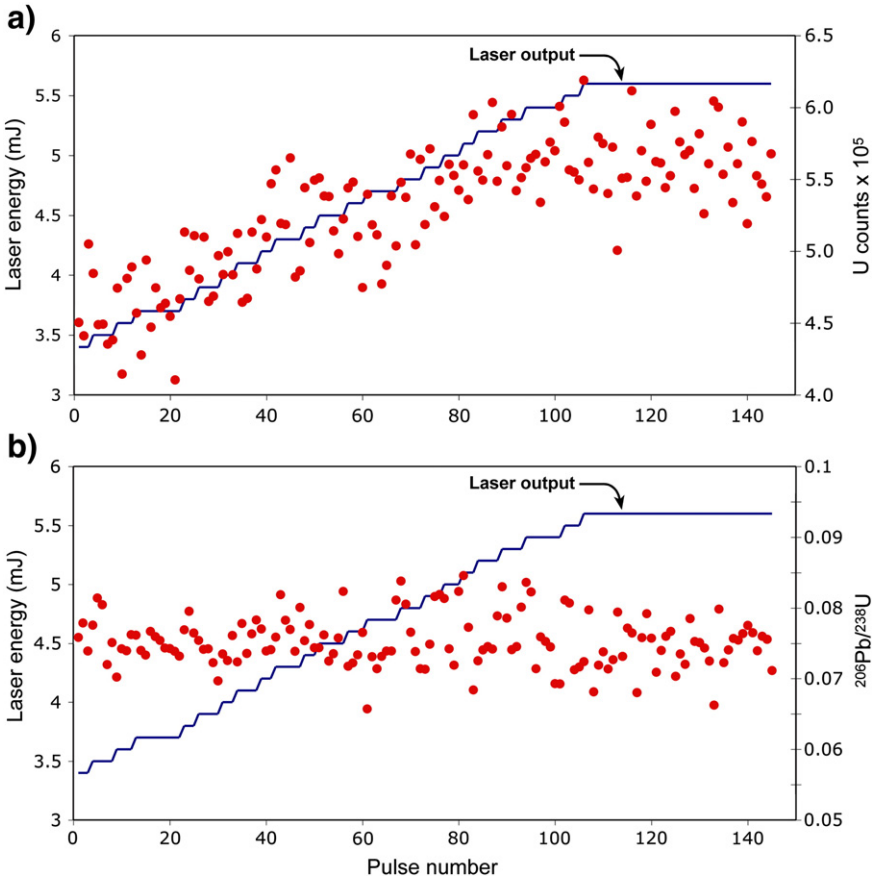

Fig. 4. Laser energy measured during repeat ablations of GJ-1 reference zircon. Laser energy was varied systematically to assess its contribution to the overall measurement uncertainty and reproducibility. a) Total uranium counts, and b) measured $^{206}Pb/^{238}U$ ratio. Variations in laser energy do not correlate to either changes in the measured ratio or the reproducibility of the measured ratio.

theory, result in lower counting statistics uncertainty for each individual analysis because the area under the curve is typically greater and therefore more counts are recorded than for the T or bulb setups. However, we elected to use just the mixing bulb configuration for three reasons: 1) it permits a shorter washout time, 2) developing an algorithm to automatically detect the baseline is more difficult

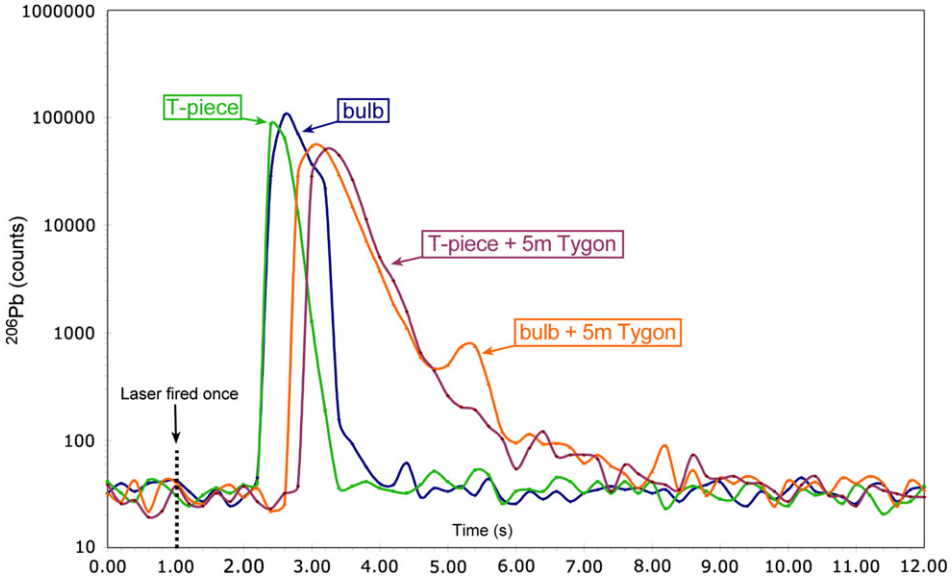

Fig. 5. Results of four different sample transport tubing experiments. 'T-piece': setup in which Ar was added to the analyte + He mixture at a Teflon T-joint approximately ~20 cm (half way) between the outlets of the cell and the ICP torch. 'Bulb': setup in which Ar was added to analyte + He mixture in a glass mixing bulb (a 25 mm diameter × 70 mm glass cylinder approximately ~20 cm (half way) between the outlets of the cell and the ICP torch. Above two configurations were tested with (labeled) and without 5 m of Teflon-lined Tygon tubing between the Ar input and the torch. Curves are mean values of 10 repeat ablations of the GJ-1 reference zircon. The laser was fired once at the 1.0-second point.

in the 'bulb + 5 m Tygon' setup because of signal variability; 3) the 'bulb + 5 m Tygon' or 'T + 5 m Tygon' configurations resulted in a slightly worse reproducibility for repeat sets of analyses.

4.2.1. Accuracy and reproducibility of reference materials—zircon

To monitor long-term data accuracy, secondary reference zircons "GJ-1" (608.4 ± 0.4 Ma $^{207}Pb/^{206}Pb$ ID-TIMS age, (Jackson et al., 2004) and 601.7 ± 1.3 Ma $^{206}Pb/^{238}U$ ID-TIMS age; (*Condon*, unpublished data) and Plešovice (337.13 ± 0.37 Ma $^{206}Pb/^{238}U$ ID-TIMS age, Sláma et al., 2008)) were analyzed repeatedly over a 12-month period. Data were normalized to a primary reference zircon, "91500" (1062.4 ± 0.4 Ma $^{206}Pb/^{238}U$ isotope dilution thermal ionization mass spectrometry (ID-TIMS) age, (Wiedenbeck et al., 1995)). Over the 12-month period, GJ-1 and Plešovice give weighted mean $^{206}Pb/^{238}U$ dates of 599.6 ± 0.7 Ma (2SE, MSWD = 1.1, n = 287) and 338.2 ± 0.5 (2 SE, MSWD = 1.5, n = 287), respectively (Fig. 6a–f, Table 1 in online

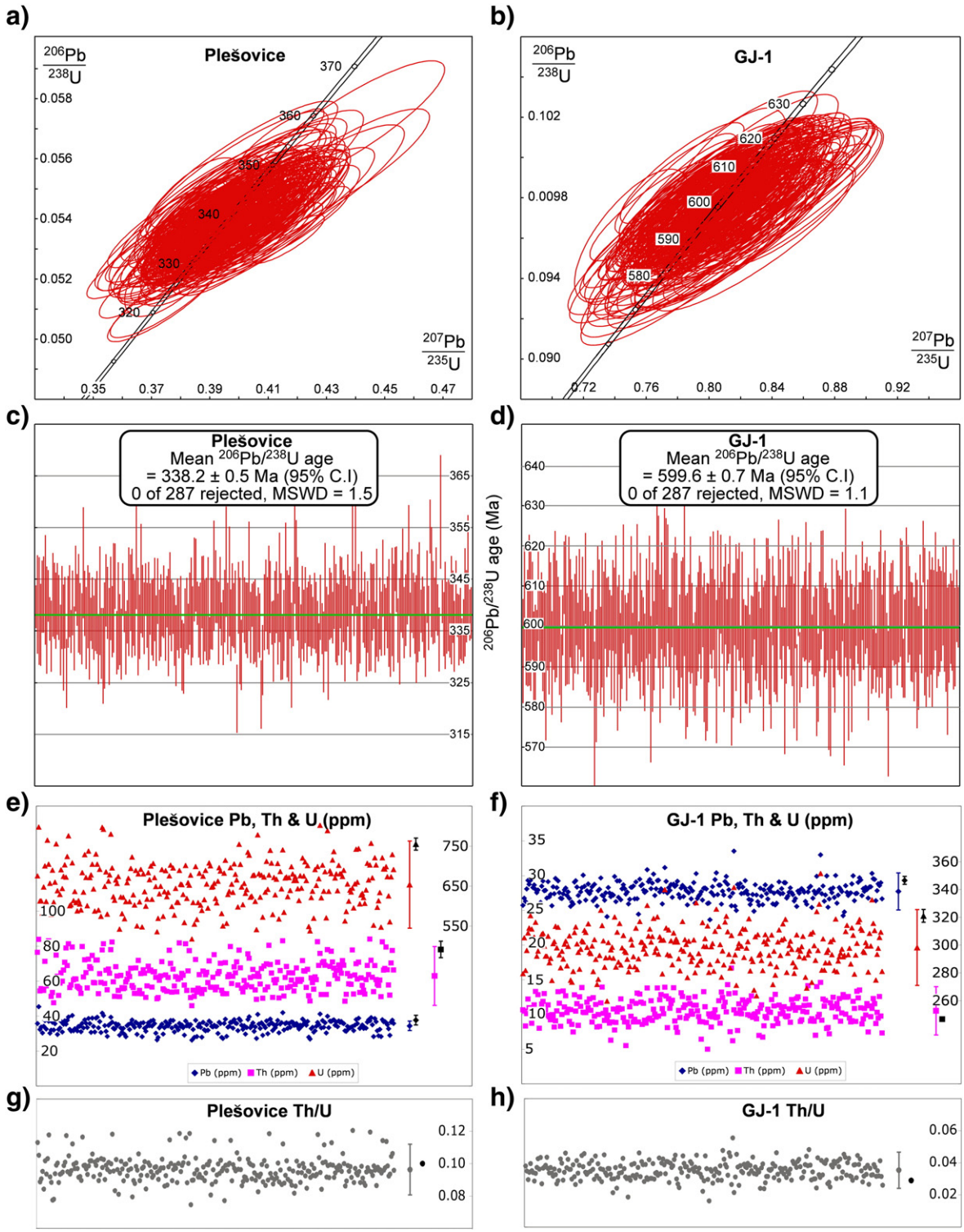

Fig. 6. Isotopic and elemental concentration data for Plešovice and GJ-1 reference zircons. a–b) Wetherill concordia diagrams, c–d) weighted mean $^{206}Pb/^{238}U$ plots for Plešovice and GJ-1, e–f) Pb (blue diamonds), Th (pink squares), and U (red triangles) concentration data, g–h) Th/U ratios. In e–h colored lines at right of plots are mean and uncertainty (2σ) of data. Black lines represent mean and uncertainty (2σ) of published values.

Appendix). The mean uncertainty on individual $^{206}Pb/^{238}U$ dates is 2.2% (2σ) for both GJ-1 and Plešovice. The U, Th and Pb concentrations and Th/U ratio for each analysis was also calculated via the method outlined above. Fig. 6g–h demonstrates that the long-term mean of each elemental concentration is within uncertainty of published values (Sláma et al., 2008; Liu et al., 2010) and each individual measurement is accurate to within approximately 5%.

4.2.2. Reproducibility of reference materials—monazite

A similar data set was collected on secondary reference monazites "Manangotry" (552.9 Ma $^{206}Pb/^{238}U$, 554 Ma $^{207}Pb/^{206}Pb$ID-TIMS ages, (Horstwood et al., 2003)) and FC1 (55.6 ± 0.4 Ma $^{206}Pb/^{238}U$, ID-TIMS age, (Horstwood et al., 2003)). Data were normalized to a primary reference monazite, "44069" (424.9 ± 0.4 Ma $^{206}Pb/^{238}U$ (ID-TIMS) age, (Aleinikoff et al., 2006)). Over a 6-month period, Manangotry and FC1 yielded weighted mean $^{206}Pb/^{238}U$ dates of 554.3 ± 2.2 Ma (2SE, MSWD = 1.9, 8 of 200 analyses rejected) and 56.9 ± 0.2 (2SE, MSWD = 2.2, 4 of 133 analyses rejected), respectively (Fig. 7a–b). The SS-LA-ICPMS FC1 date is too old by 0.7 Ma (1.2%), which we attribute to minor age heterogeneity in FC-1 and the possibility of a minor common lead that would drive the age to an older value. Weighted mean $^{208}Pb/^{232}Th$ dates for Manangotry and FC1 are 540.1 ± 1.8 Ma (2SE, MSWD = 2.6, 8 of 200 analyses rejected) and 55.6 ± 0.3 (2SE, MSWD = 2.8, 7 of 133 analyses rejected), respectively (Fig. 7c–d). The mean uncertainty on individual Manangotry and FC1 $^{206}Pb/^{238}U$ dates is 2.9 and 3.5% (2σ) and 4.0 and 3.2% for individual $^{208}Pb/^{232}Th$ dates. The U, Th and Pb concentrations and Th/U ratio for each analysis was also calculated via the method outlined above. Fig. 7e–h demonstrates that the long-term mean of each elemental concentration is within uncertainty of our unpublished electron probe microanalyzer (EPMA) values (plotted in black) and that each individual measurement is accurate to within approximately 10%.

4.3. U–Pb detrital zircon geochronology

As a case study exploring the application of the single shot method to detrital zircon U–Pb geochronology, aliquots of zircon from a clastic sediment were prepared and analyzed by 'conventional' LA-ICPMS and SS-LA-ICPMS methods. A 5 kg sample (Tsp) was selected from near the base of the Sespe Formation, in the Santa Ynez Mountains north of Santa Barbara, CA, (34.4603°, −119.6882°, 370 m a.s.l). The Sespe Formation forms part of folded and faulted Cretaceous through Pleistocene sedimentary strata that make up the western portion of the Transverse Range in California. The Sespe consists of a 670–1380 m-thick sequence of arkosic sandstone, siltstone, and conglomerate that overlies the Coldwater Formation and is, in turn, depositionally overlain by the Vaqueros Formation. Biostratigraphic data suggest that the Sespe Formation was deposited between 37 and 24 Ma (Dibblee, 1966).

This sample was selected because it potentially contains zircons of a variety of ages as well as differences in U (and Pb) concentrations; as such it provides a good test of the utility of the single shot method to detrital zircon studies.

4.3.1. Conventional laser ablation protocol

As outlined above, the conventional laser ablation protocol employed at UCSB for zircon involves two cleaning shots followed by 25 s of continuous laser pulsing at a spot diameter of 24 μm, a frequency of 4 Hz (100 shots) and 2.7 J/cm^2 fluence.

For zircon analyses, 91500 zircon was used as a primary reference material to monitor and correct for mass bias and Pb/U fractionation. To monitor data accuracy, secondary reference zircons GJ-1and Plešovice were analyzed concurrently (once every 10 unknowns) and corrected for mass bias and fractionation based on measured isotopic ratios of the primary reference material. Repeat analyses of GJ-1 and Plešovice during the analytical session give a weighted mean $^{206}Pb/^{238}U$ date of 603.6 ± 2.5 (2SE, MSWD = 1.1, n = 13) and 337.4 ± 1.6 (2SE, MSWD = 0.8, n = 13), respectively.

A total of 120 unknowns were analyzed–a run time of approximately 2 h–enabling the identification of components making up >5% of the total population at the 95% confidence interval (Vermeesch, 2004) (Table 1 in online Appendix). A 15% discordance cut-off was applied to the data, resulting in the rejection of 26 analyses. The remaining zircons have a range of $^{206}Pb/^{238}U$ dates from 70 Ma to 1815 Ma, U concentrations from 25 to 2240 ppm (mode ~400 ppm) and Pb concentrations of 1–1750 ppm (mode ~70 ppm). Rejecting 5 analyses with uncertainties >10% (with a significant common-lead component indicated by $^{206}Pb/^{204}Pb$ ratios), the mean $^{206}Pb/^{238}U$ 2σ uncertainty for these data is 2.21 ± 0.61 (2SD). Plotted on a probability density function (PDF) (Fig. 8) the sample contains prominent age clusters at 1.55–1.8 Ga, 1.4 Ga, and 100–250 Ma.

4.3.2. Single shot ablation protocol

As with the conventional ablation protocol, 120 unknowns were analyzed, bracketed by a primary and two secondary reference zircons every 10 unknowns. Each unknown and reference material was ablated with two cleaning shots before analysis. The total run time for cleaning and analysis was approximately 20 min. Repeat analyses of GJ-1 and Plešovice give weighted mean $^{206}Pb/^{238}U$ age of 597.4 ± 4.4 (2SE, MSWD = 1.01, n = 14) and 336.3 ± 3.1 (2SE, MSWD = 1.3, n = 14), respectively.

Twenty-one analyses were rejected as being ≥15% discordant. The remaining zircons have a range $^{206}Pb/^{238}U$ dates from 90 Ma to 1750 Ma, U concentrations from 2 to 3620 ppm (mode ~390 ppm) and Pb concentrations of 2–387 ppm (mode ~64 ppm) (Table 1 in online Appendix), similar to those concentrations generated by the conventional method. Rejecting 8 analyses with uncertainties >10%, the mean $^{206}Pb/^{238}U$ 2σ uncertainty for these data is 2.9 ± 0.4 (2 SD). This compares to 2.2% for the conventional ablation protocol. This minor reduction in precision is balanced by the fact that the SS-LA-ICPMS method consumes approximately 70× less material compared to the conventional ablation protocol and requires 1/6th of the analysis time.

The sample contains the same prominent age clusters at 1.55–1.8 Ga, 1.4 Ga, and 100–250 Ma as the conventional laser ablation data (Fig. 8). The similarity of the results generated by the two analytical methods was assessed with the Kolmogorov–Smirnov (K–S) statistical test. The K–S test evaluates the null hypothesis that two data distributions are from the same population (Press et al., 2002). It achieves this by comparing the maximum probability distance between the cumulative distribution functions (CDFs) of the two distributions. A critical distance can then be defined for a given confidence interval beyond which the distributions are unlikely to be drawn from the same population. To be 95% confident that two populations are not statistically different, the Probability, *P*, value must exceed 0.05. Comparing the data from the two methods results in a maximum difference between the cumulative distributions, *D*, of 0.1894 with a corresponding *P* of 0.055, the two samples are indistinguishable using the K–S test.

4.4. U–Th/Pb detrital monazite geochronology

Because zircon has a relatively high closure temperature and is resistant to dissolution and re-setting, U–Pb detrital zircon ages from an orogenic belt dominantly record igneous and high temperature metamorphic episodes, but are less successful in quantifying other orogenic processes, including rates of crustal burial and thickening, low- to moderate-temperature metamorphism and exhumation. The potential of monazite to record many processes that zircon does not, makes it an ideal complementary tracer of orogenic development (e.g. Parrish, 1990).

To test whether the SS-LA-ICPMS method is capable of producing precise and accurate monazite age distributions, a ~3 kg sample of modern river sand (sample PC2) was collected from the edge of the active channel

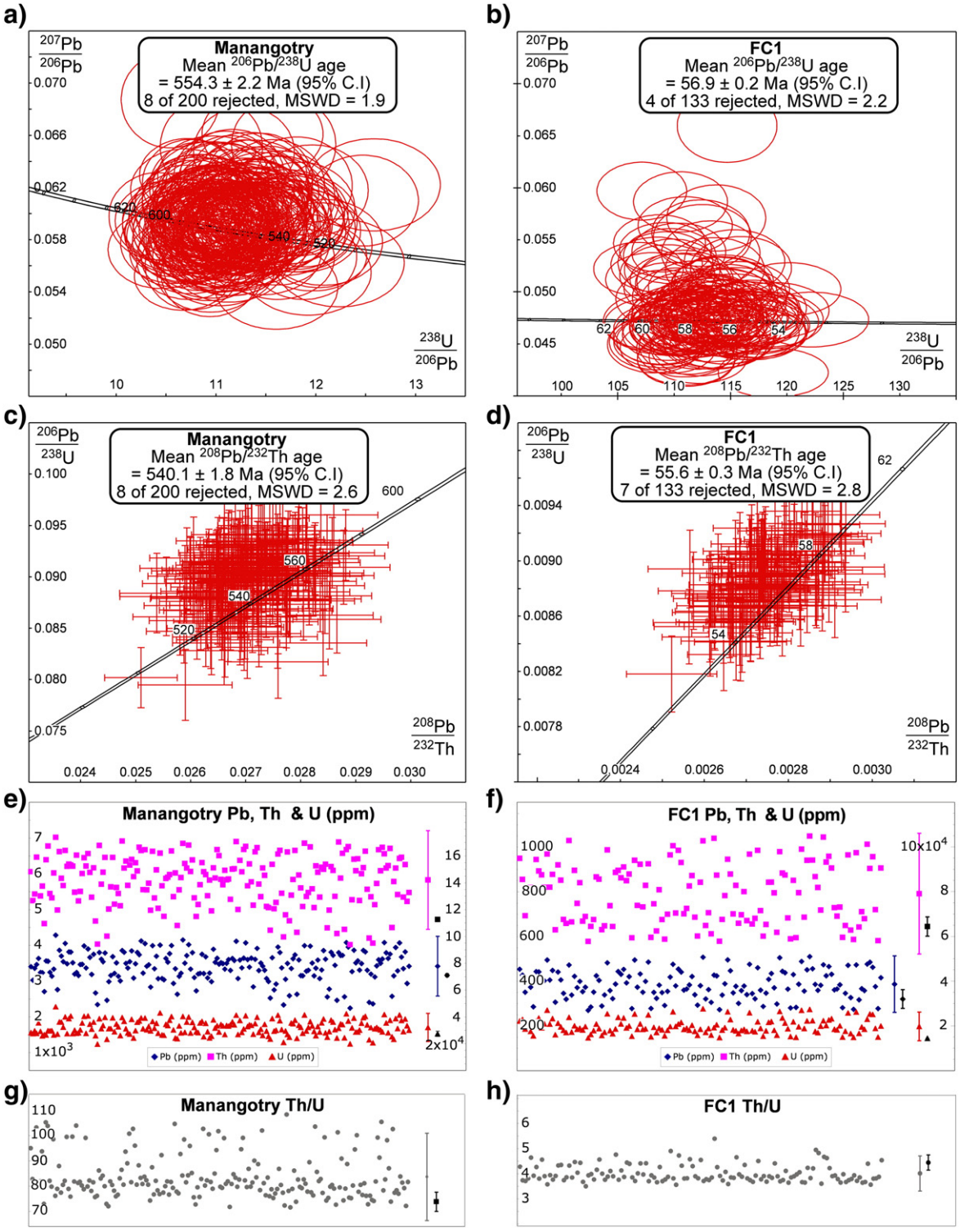

Fig. 7. Isotopic and elemental concentration data for Manangotry and FC1 reference monazites. a–b) Tera–Wasserburg concordia diagrams, c–d) Th/Pb vs. U/Pb concordia diagram, e–f) Pb (blue diamonds), Th (pink squares), and U (red triangles) concentration data, g–h) Th/U ratio data. In e–h colored lines at right of plots are mean and uncertainty (2σ) of datasets. Black lines represent mean and uncertainty (2σ) of unpublished electron probe microanalyzer values.

in the Arun river (Phung Chu) in southern Tibet (28.0994°, 87.3592°, 3575 m a.s.l). As with the zircon sample, this sample was selected because the source region contains a variety of ages including Proterozoic (~1.8 Ga), Paleozoic (~480–500 Ma) and Tertiary (~40–10 Ma) (see Cottle et al., 2007, 2009b, 2009c for details of the regional tectonic and geochronologic frameworks) and therefore presents a good test of the single-shot method at a variety of ages as well as Pb, U, and Th concentrations.

4.4.1. Conventional laser ablation protocol

The conventional laser ablation protocol employed at UCSB for monazite involves two cleaning shots followed by 25 s of continuous

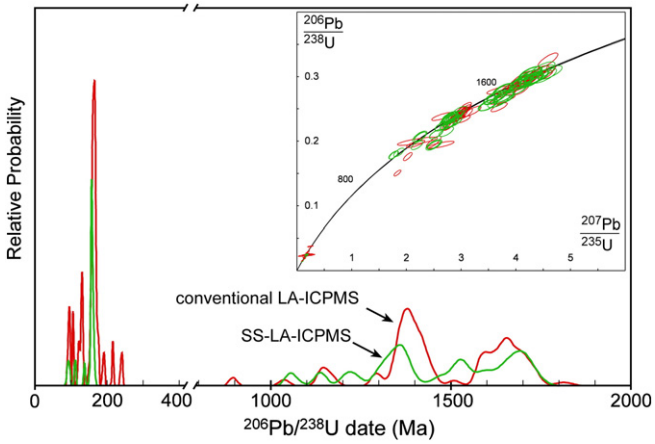

Fig. 8. Probability density function (PDF) for detrital zircons from a sample of the Sespe Formation (34.4603°, −119.6882°, 370 m a.s.l). Green lines and ellipses are SS-LA-ICPMS analyses, red lines and ellipses are conventional LA-ICPMS analyses. Inset is a Wetherill concordia of data that are <15% discordant.

laser pulsing at a spot diameter of 7 μm, a frequency of 4 Hz (100 shots) and 2.7 J/cm^{2}fluence.

For monazite analyses, '44069' was used as a primary reference material to monitor and correct for mass bias and Pb/U and Pb/Th fractionation. To monitor data accuracy, secondary reference monazites Manangotry and FC1 were analyzed concurrently (once every 10 unknowns) and corrected for mass bias and fractionation based on the measured isotopic ratios of the primary reference material. Repeat analyses of Manangotry and FC1 during the analytical session give a weighted mean $^{208}Pb/^{232}Th$ date of 532.4 ± 3.4 (2SE, MSWD = 1.4, n = 15) and 53.6 ± 0.4 (2SE, MSWD = 1.7, n = 16), respectively.

No rejection criterion based on discordance was applied to the monazite data. The $^{207}Pb/^{235}U$ dates may be imprecise because of low counts of ^{207}Pb, they may also be inaccurate because any initial ^{207}Pb will potentially have a significant influence on the calculated date. In addition, the $^{206}Pb/^{238}U$ and $^{207}Pb/^{206}Pb$ dates cannot be used to assess discordance relative to the $^{208}Pb/^{232}Th$ date because monazites typically contain 'excess' ^{206}Pb, as a result of non-equilibrium incorporation of ^{230}Th (an intermediate product in the ^{238}U decay scheme) (Schärer, 1984). This leads to $^{206}Pb/^{238}U$ dates that are too old by as much as 50% (Cottle et al., 2009b).

A total of 120 unknowns were analyzed (Table 2 in online Appendix). Plotted on a probability density function (PDF) (Fig. 9) the analyzed monazites have a range of $^{208}Pb/^{232}Th$ dates with prominent age clusters at ~12.5, 16 and 32 Ma. Individual $^{208}Pb/^{232}Th$ dates have a mean uncertainty of 2.4% (2σ). The median U and Th concentrations for all analyses are 6190 and 49,700 ppm, respectively.

4.4.2. Single shot ablation protocol

As with the conventional ablation protocol, 120 unknowns were analyzed bracketed by a primary and two secondary reference monazites for every 10 unknowns (Table 2 in online Appendix). Repeat analyses of Manangotry and FC1 give weighted mean $^{208}Pb/^{232}Th$ dates of 524.1 ± 7.6 (2σ, MSWD = 1.7, n = 16) and 53.4 ± 0.9 (2σ, MSWD = 1.3, n = 16), respectively. The monazite aliquot analyzed by SS-LA-ICPMS has similar age peaks to the conventional analyses at ~13, 17 and 30 Ma (Fig. 9). Individual $^{208}Pb/^{232}Th$ date determinations have a mean uncertainty of 4.9% (2σ). Median U and Th concentrations are 7406 and 61,527 ppm, respectively. Comparing the data from the two methods (conventional

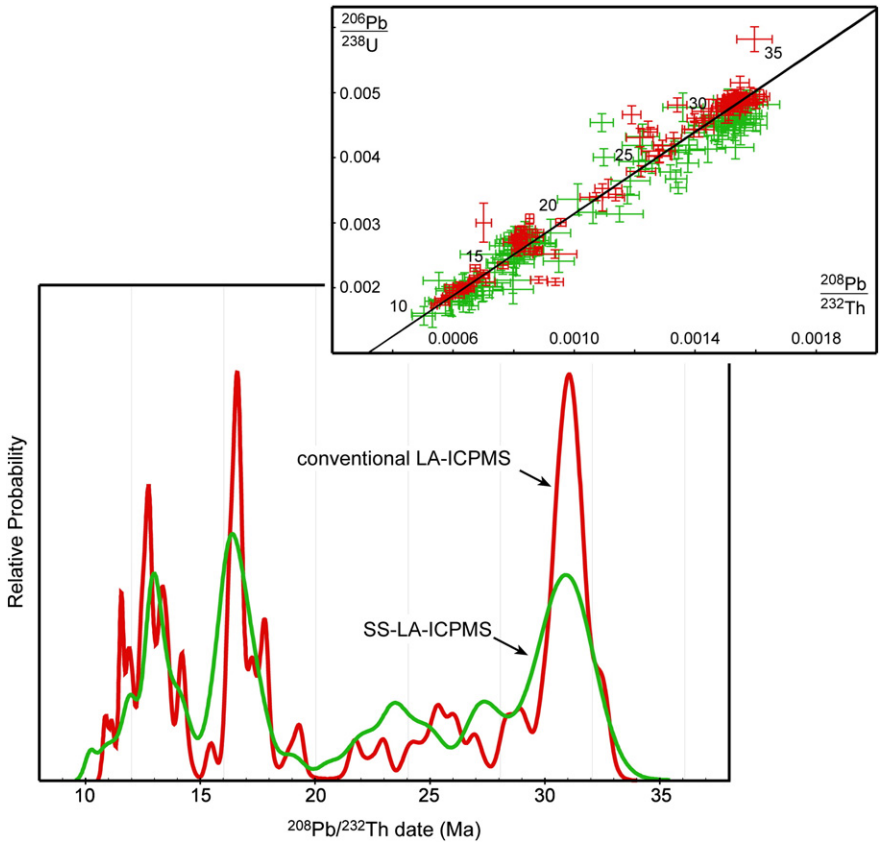

Fig. 9. Probability density function (PDF) for detrital monazites from a modern sediment sample from the Phung Chu river (28.0994°, 87.3592°, 3575 m a.s.l). Green lines and ellipses are SS-LA-ICPMS analyses, red lines and ellipses are conventional LA-ICPMS analyses. Inset is a Pb/Th vs. Pb/U of data that are <15% discordant.

LA-ICPMS vs. SS-LA-ICPMS) using the K–S statistic results in a maximum difference between the cumulative distributions, *D*, of 0.1157 with a corresponding *P* of: 0.372, it therefore passes the K–S test (*P* value must be >0.05 to pass) and the two samples can be considered identical within uncertainty.

5. Discussion

5.1. Accuracy and precision of SS-LA-ICPMS

Typical individual, single-shot $^{206}Pb/^{238}U$ measurements of zircon reference materials have uncertainties ranging from 2 to 5% (2SE), whereas individual single-shot $^{208}Pb/^{232}Th$ measurements of monazite reference materials range from 2.5 to 3.7% (2SE). The uncertainty on the long-term weighted mean $^{206}Pb/^{238}U$ dates is 0.12%, 0.15%, 0.4% and 0.4% for GJ-1, Plešovice, Manangotry, and FC1, respectively. In contrast, the uncertainty on the long-term weighted mean $^{208}Pb/^{232}Th$ dates is 0.3% and 0.5% for the Manangotry and FC1 monazites, respectively. The long-term weighted-mean uncertainties provide the lower limit for the precision of this technique; and while these data demonstrate, that in theory it is possible to measure an individual sample to sub-percent precision, we take the short-term reproducibility of the reference materials as a more realistic assessment with which routine age determinations can be made.

Through primary-reference error propagation, as described in Section 3.4, the MSWD for repeat $^{206}Pb/^{238}U$ measurements of reference zircons within an analytical session is consistently close to unity. Likewise, the MSWD for the long-term zircon datasets are also close to one. The MSWD for the $^{208}Pb/^{232}Th$ monazite datasets is slightly greater than one indicating scatter in the data or that the uncertainties are underestimated. Because the error propagation technique appears to work well for zircons, the higher MSWD for monazites is likely a result of minor compositional/age heterogeneities in the reference monazites and/or ionization variability of thorium compared to uranium, rather than an under-estimation of the analytical uncertainty. Taken as a whole, our data suggest that the error propagation technique outlined above suitably approximates the uncertainty associated with this technique and can be applied to sets of unknowns.

In terms of accuracy, the mean $^{206}Pb/^{238}U$ date obtained for GJ-1 reference zircon is well within the uncertainty of the ID-TIMS value, whereas the SS-LC-ICPMS $^{206}Pb/^{238}U$ date for Plešovice is too old, requiring the addition of 0.06% uncertainty to be statistically indistinguishable from the published value of Sláma et al. (2008). The mean $^{206}Pb/^{238}U$ dates obtained for Manangotry and FC1 are within 0.2% uncertainty of the ID-TIMS values. None of the reference monazites analyzed in this study have independently determined high-precision $^{208}Pb/^{232}Th$ dates. Although this precludes a quantitative assessment of the accuracy of the SS-LA-ICPMS $^{208}Pb/^{232}Th$ dates, the mean $^{208}Pb/^{232}Th$ date for FC-1 agrees with the ID-TIMS $^{206}Pb/^{238}U$ value. The $^{208}Pb/^{232}Th$ date obtained for Manangotry by SS-LA-ICPMS is ~3% younger than the ID-TIMS $^{206}Pb/^{238}U$ date, but similar to that routinely obtained by conventional LA-ICPMS analysis in our laboratory. Paquette and Tiepolo (2007) and Kohn and Vervoort (2008) also noted a similar discrepancy between $^{206}Pb/^{238}U$ and $^{208}Pb/^{232}Th$ dates obtained from Manangotry. We remain uncertain whether this discrepancy is a result of age heterogeneity or disequilibrium between the Pb–U and Pb–Th systems.

In the study of Cottle et al. (2009a), the relatively imprecise and/or inaccurate concentration data were inferred to result from variations in shot-to-shot laser irradiance (using a solid state 193 mn laser system). In contrast, the concentration data produced in this study are more precise and have accuracies comparable to conventional LA-ICPMS methods designed for isotope ratio analysis. This suggests that the observed 8% variation in shot-to-shot energy output does not directly translate into an equivalent variation in ablation yield from the sample. Furthermore, our data (Fig. 4) indicate that the contribution of variations in pulse-to-pulse laser energy to the uncertainty of LA-ICPMS analyses is minor. Neither the absolute value nor the reproducibility of the obtained ratios appears to change significantly when laser energy is varied. This implies that variations in laser energy do not contribute significantly to the overall reproducibility of this technique.

5.2. Application to detrital accessory phase geochronology

Analyses of natural detrital zircon and monazites provide further support for the validity of the SS-LA-ICPMS method. Kolmogorov–Smirnov (K–S) statistical tests on detrital zircon and monazite samples run both by conventional LA-ICPMS and SS-LA-ICPMS indicate that there is no resolvable difference in the age distributions at the 95% confidence level. In both cases the samples are essentially identical, and produce age spectra that are equivalent. We therefore conclude that this method can be routinely employed in detrital accessory phase geochronology.

Depending on the setup employed, a conventional LA-ICPMS protocol consists of 15–40 s of ablation and 15–30 second wait time while the signal returns to baseline. This means that it takes ~2 h to analyze 120 unknowns and the couple of a dozen required reference materials. With the SS-LA-ICPMS method the time required to obtain the same dataset can be reduced to ~20 min with only a modest increase in individual data point uncertainty (from ~2% to ~4%) and no loss of sub-population identification (for components >5% of the total at 95% confidence) compared to conventional LA-ICPMS methods. Similarly, the SS-LA-ICPMS method can analyze ~300 unknowns plus reference zircons per hour, making it the pre-eminent tool to rapidly screen large numbers of zircons to find the youngest grains within a sample prior to high-precision ID-TIMS analysis. This tool may find particular use in chronostratigraphic studies where zircons from ash beds can be rapidly screened to avoid analyzing inherited zircons but also identify those zircons that fall within the youngest population. In addition, the SS-LA-ICPMS method has the potential to be a useful tool to rapidly screen large numbers of zircons from Archean sediments to locate relatively rare Hadean-age grains. Because, of their low abundance–the Jack Hills quartzite contains only ~7% > 3.8 Ga–Holden et al. (2009) estimate needing to screen between 150,000 and 300,000 grains from such rocks to find enough Hadean zircons for a systematic study. Screening with SS-LA-ICPMS has the potential to be complimentary to the rapid analysis methods developed for SHRIMP by workers such as Holden et al. (2009).

6. Conclusions

The SS-LA-ICPMS method is capable of consistently producing ages and concentration data on secondary reference zircons and monazites that are within uncertainty of the accepted ID-TIMS/reference values. Analyses of detrital zircon and monazite samples by both conventional LA-ICPMS and SS-LA-ICPMS yield statistically identical results, indicating that this method is suitable for routine application in detrital accessory phase studies and as a screening tool prior to high precision analysis.

Supplementary data to this article can be found online at http://dx.doi.org/10.1016/j.chemgeo.2012.09.035.

Acknowledgments

This material is based upon work supported by the National Science Foundation under Grant No. (NSF-EAR-1050043), the Hellman Foundation, and the University of California, Santa Barbara. We thank two anonymous reviewers for their constructive comments.

References

Aleinikoff, J.N., Schenck, W.S., Plank, M.O., Srogi, L., Fanning, C.M., Kamo, S.L., Bosbyshell, H., 2006. Deciphering igneous and metamorphic events in high-grade rocks of the Wilmington Complex, Delaware: morphology, cathodoluminescence and backscattered electron zoning, and SHRIMP U–Pb geochronology of zircon

and monazite. Geological Society of America Bulletin 118, 39–64 http://dx.doi.org/10.1130/B256591.
Amelin, Y., Zaitsev, A.N., 2002. Precise geochronology of phoscorites and carbonatites: The critical role of U-series disequilibrium in age interpretations, Geochimica Cosmochimica Acta 66, 2399–2419.
Cottle, J.M., Jessup, M.J., Newell, D.L., Searle, M.P., Law, R.D., Horstwood, M.S.A., 2007. Structural insights into the early stages of exhumation along an orogen-scale detachment: the South Tibetan Detachment System, Dzakaa Chu section, Eastern Himalaya. Journal of Structural Geology 29, 1781–1797 http://dx.doi.org/10.1016/j.jsg.2007.08.007.
Cottle, J.M., Horstwood, M.S.A., Parrish, R.R., 2009a. A new approach to single shot laser ablation analysis and its application to in situ Pb/U geochronology. Journal of Analytical Atomic Spectrometry 24, 1355–1363 http://dx.doi.org/10.1039/b821899d.
Cottle, J.M., Searle, M.P., Horstwood, M.S.A., Waters, D.J., 2009b. Timing of mid-crustal metamorphism, melting and deformation in the Mt. Everest region of southern Tibet revealed by U(–Th)–Pb geochronology. Journal of Geology 117, 643–664 http://dx.doi.org/10.1086/605994.
Cottle, J.M., Jessup, M.J., Newell, D.L., Horstwood, M.S.A., Searle, M.P., Parrish, R.R., Waters, D.J., Searle, M.P., 2009c. Geochronology of granulitized eclogite from the Ama Drime Massif: implications for the tectonic evolution of the South Tibetan Himalaya. Tectonics 28, TC1002 http://dx.doi.org/10.1029/2008TC002256.
Dibblee, T.W., 1966. Geology of the central Santa Ynez Mountains, Santa Barbara County, California. California Division of Mines and Geology, Bulletin 186, 99p.
Eggins, S.M., Grün, R., McCulloch, M.T., Pike, A.W.G., Chappell, J., Kinsley, L., Mortimer, G., Shelley, M., Murray-Wallace, C.V., Spötl, C., Taylor, L., 2005. In situ U-series dating by laser ablation multi-collector ICP-MS: new prospects for Quaternary geochronology. Quaternary Science Reviews 24, 2523–2538 http://dx.doi.org/10.1016/j.quascirev.2005.07.006.
Eggins, S.M., Kinsley, L.P.J., Shelley, J.M.G., 1998. Deposition and element fractionation processes during atmospheric pressure laser sampling for analysis by ICP-MS. Applied Surface Science 127–129, 278–286 http://dx.doi.org/10.1016/S0169-4332(97)00643-0.
Gehrels, G., Valencia, V.A., Ruiz, J., 2008. Enhanced precision, accuracy, efficiency, and spatial resolution of U–Pb ages by laser ablation-multicollector-inductively coupled plasma-mass spectrometry. Geochemistry, Geophysics, Geosystems 9 (3), Q03017 http://dx.doi.org/10.1029/2007GC001805.
Holden, P., Lanc, P., Ireland, T.R., Harrison, T.M., Foster, J.J., Bruce, Z., 2009. Mass-spectrometric mining of Hadean zircons by automated SHRIMP multi-collector and single-collector U/Pb zircon age dating: the first 100,000 grains. International Journal of Mass Spectrometry 286, 53–63 http://dx.doi.org/10.1016/j.ijms.2009.06.007.
Horstwood, M.S.A., Foster, G.L., Parrish, R.R., Noble, S.R., Nowell, G.M., 2003. Common-Pb corrected in situ U-Pb accessory mineral geochronology by LA-MC-ICP-MS. Journal of Analytical Atomic Spectrometry 18, 837–846 http://dx.doi.org/10.1039/b304365g.
Jackson, S.,Pearson, N., Griffin, W., 2001. In situ isotope ratio determination using laser ablation (LA)-magnetic sector-ICP-MS, in Laser-Ablation-ICPMS in the Earth Sciences: Principles and Applications, Short Course Ser., vol. 29, edited by P. Sylvester, pp. 105–120, Mineral. Assoc. of Can., St John's, Newfoundland.
Jackson, S.E., Pearson, N.J., Griffin, W.L., Belousova, E.A., 2004. The application of laser ablation-inductively coupled plasma-mass spectrometry to in situ U/Pb zircon geochronology. Chemical Geology 211, 47–69 http://dx.doi.org/10.1016/j.chemgeo.2004.06.017.
Jaffey, A.H., Flynn, K.F., Glendenin, L.E., Bentley, W.C., Essling, A.M., 1971. Precision measurement of the half-lives and specific activities of U235 and U238. Physical Reviews C 4, 1889–1906 http://dx.doi.org/10.1103/PhysRevC.4.1889.
Johnston, S., Gehrels, G., Valencia, V., Ruiz, J., 2009. Small-volume U-Pb zircon geochronology by laser ablation-multicollector-ICP-MS. Chemical Geology 259, 218–229 http://dx.doi.org/10.1016/j.chemgeo.2008.11.004.
Kohn, M.J., Vervoort, J.D., 2008. U-Th-Pb dating of monazite by single-collector ICP-MS: Pitfalls and potential. Geochemistry, Geophysics, Geosystems 9, Q04031.
Košler, J., Fonneland, H., Sylvester, P., Turbrett, M., Pedersen, R.-B., 2002. U–Pb dating of detrital zircons for sediment provenance studies—a comparison of laser ablation ICPMS and SIMS techniques. Chemical Geology 182, 605–618 http://dx.doi.org/10.1016/S0009-2541(01)00341-2.
Liu, Y., Hu, Z., Zong, K., Gao, C., Gao, S., Xu, J., Chen, H., 2010. Reappraisement and refinement of zircon U–Pb isotope and trace element analyses by LA-ICP-MS. Chinese Science Bulletin 55, 1535–1546 http://dx.doi.org/10.1007/s11434-010-3052-4.
Ludwig, K.R., 2012. User's Manual for Isoplot 3.75, A Geochronological Toolkit for Microsoft Excel, Berkeley Geochronology Center Special Publication No. 5.
Paquette, J.-L., Tiepolo, M., 2007. High resolution (5 μm) U–Th–Pb isotope dating of monazite with excimer laser ablation (ELA)-ICPMS. Chemical Geology 240, 222–237 http://dx.doi.org/10.1016/j.chemgeo.2007.02.014.
Parrish, R.R., 1990. U–Pb dating of monazite and its application to geological problems. Canadian Journal of Earth Sciences 27, 1431–1450 http://dx.doi.org/10.1139/e90-152.
Paton, C., Woodhead, J.D., Hellstrom, J.C., Hergt, J.A., Greig, A., Mass, R., 2010. Improved laser ablation U–Pb zircon geochronology through robust downhole fractionation correction. Geochemistry, Geophysics, Geosystems 11, Q0AA06 http://dx.doi.org/10.1029/2009GC002618.
Pettke, T., Oberli, F., Audétat, A., Wiechert, U., Harris, C.R., Heinrich, C.A., 2011. Quantification of transient signals in multiple collector inductively coupled plasma mass spectrometry: accurate lead isotope ratio determination by laser ablation of individual fluid inclusions. Journal of Analytical Atomic Spectrometry 26, 475–492 http://dx.doi.org/10.1039/C0JA00140F.
Press, W.H., Teukolsky, S.A., Vetterling, W.T., Flannery, B.P., 2002. Numerical Recipes: The Art of Scientific Computing, 2nd ed. Cambridge University Press, p. 997.
Schärer, U., 1984. The effect of initial ^{230}Th disequilibrium on young U–Pb ages—the Makalu Case, Himalaya. Earth and Planetary Science Letters 67, 191–204 http://dx.doi.org/10.1016/0012-821X(84)90114-6.
Sláma, J., et al., 2008. Plešovice zircon—a new natural reference material for U–Pb and Hf isotopic analysis. Chemical Geology 249, 1–35 http://dx.doi.org/10.1016/j.chemgeo.2007.11.005.
Steiger, R.H., Jäger, E., 1977. Subcommission on geochronology, convention on the use of decay constants in geo- and cosmochronology. Earth and Planetary Science Letters 36, 359–362 http://dx.doi.org/10.1016/0012821X(77)90060-7.
Vermeesch, P., 2004. How many grains are needed for a provenance study? Earth and Planetary Science Letters 224, 441–451 http://dx.doi.org/10.1016/j.epsl.2004.05.037.
Wiedenbeck, M., et al., 1995. Three natural zircon standards for U–Th–Pb, Lu–Hf, trace element, and REE analyses. Geostandards Newsletter 19 (1), 1–23 http://dx.doi.org/10.1111/j.1751-908X.1995.tb00147.x.
Zack, T., Sockli, D.F., Luvizotti, G.L., Barth, M.G., Belousova, E., Wolfe, M.R., Hinton, R.W., 2011. In-situ U/Pb rutile dating by LA-ICP-MS: ^{208}Pb correction and prospects for geological applications. Contributions to Mineralogy and Petrology 162 (3), 515–530 http://dx.doi.org/10.1007/s00410-011-0609-4.